

# 3D simulations of globules and pillars formation around HII regions: turbulence and shock curvature

P. Tremblin<sup>1</sup>, E. Audit<sup>1,2</sup>, V. Minier<sup>1</sup>, W. Schmidt<sup>3</sup>, and N. Schneider<sup>1</sup>

<sup>1</sup> Laboratoire AIM Paris-Saclay (CEA/Irfu - Uni. Paris Diderot - CNRS/INSU), Centre d'études de Saclay, 91191 Gif-Sur-Yvette, France

<sup>2</sup> Maison de la Simulation, CEA-CNRS-INRIA-UPS-UVSQ, USR 3441, Centre d'étude de Saclay, 91191 Gif-Sur-Yvette, France

<sup>3</sup> Institut für Astrophysik der Universität Göttingen, Friedrich-Hund-Platz 1, D-37077 Göttingen, Germany

## ABSTRACT

**Aims.** We investigate the interplay between the ionization radiation from massive stars and the turbulence inside the surrounding molecular gas thanks to 3D numerical simulations.

**Methods.** We used the 3D hydrodynamical code HERACLES to model an initial turbulent medium that is ionized and heated by an ionizing source. Three different simulations are performed with different mean Mach numbers (1, 2 and 4). A non-equilibrium model for the ionization and the associated thermal processes was used. This revealed to be crucial when turbulent ram pressure is of the same order as the ionized-gas pressure.

**Results.** The density structures initiated by the turbulence cause local curvatures of the dense shell formed by the ionization compression. When the curvature of the shell is sufficient, the shell collapse on itself to form a pillar while a smaller curvature leads to the formation of dense clumps that are accelerated with the shell and therefore remain in the shell during the simulation. When the turbulent ram pressure of the cold gas is sufficient to balance the ionized-gas pressure, some dense-gas bubbles have enough kinetic energy to penetrate inside the ionized medium, forming cometary globules. This suggests a direct relation in the observations between the presence of globules and the relative importance of the turbulence compared to the ionized-gas pressure. The probability density functions present a double peak structure when the turbulence is low relative to the ionized-gas pressure. This could be used in observations as an indication of the turbulence inside molecular clouds.

**Key words.** Stars: formation - HII regions - ISM: structure - Turbulence - Methods: numerical

## 1. Introduction

Although massive stars have a great impact on their environment, the importance of their radiative feedback on star-formation rates is still a matter of discussion. For example, Dale et al. (2005) found a slight enhancement of the star-formation activity when the radiative feedback is taken into account whereas they recently presented simulations on a scale of a giant molecular cloud with almost no impact (see Dale & Bonnell 2011). A closer look at the small scales helps addressing this question by identifying the detailed mechanisms that form the dense structures eventually leading to star formation. These structures consist mainly of pillars of gas pointing toward the ionizing source, globules detached from the parent molecular cloud, and dense clumps at the interface between the HII region and the cloud. Optical, infrared (IR), and far-IR observations, using the Hubble space telescope and the Spitzer and Herschel satellites impressively revealed these features, mainly in high-mass star-forming regions (e.g. Hester et al. 1996; Gerin et al. 2009; Deharveng et al. 2010; Schneider et al. 2010; Zavagno et al. 2010). Several models have been proposed to explain their formation. The collect and collapse scenario described by Elmegreen & Lada (1977) or shadowing instabilities in the ionization front (e.g. Williams 1999) concentrate on the formation of dense clumps at the interface. Bertoldi (1989) and Lefloch & Lazareff (1994) with the radiation driven implosion

of clumps studied the formation of globules and Mackey & Lim (2010) proposed the shadowing effect to explain the formation of pillars.

In a previous paper (Tremblin et al. (2012), paper I hereafter), we presented a new approach emphasizing the importance of the curvature of the dense shell at the edge of the HII region to explain the formation of pillars and dense clumps in the shell. When the shell is sufficiently curved, a pillar will form by the collapse of the shell on itself, while a smaller curvature will trigger lateral flows forming dense clumps and dips inside the shell. However this scenario and the previous ones presented above are rather idealized set-ups and have to be validated in more realistic situations, e.g. taking into account a turbulent molecular cloud.

Recent studies (see Mellema et al. 2006; Gritschneider et al. 2010; Arthur et al. 2011) started to concentrate on the interplay between ionization from the massive stars and the turbulence inside the molecular cloud. They found that pillars, dense clumps and globules emerge naturally in their models, however the detailed processes forming these structures are difficult to identify with the turbulence.

In the present study, we concentrate on the interplay between turbulence and ionization in the light of the detailed processes presented in paper I. We first present the numerical method used and some tests of the out-of-equilibrium ionization module, followed by three ionized turbulent simulations at different mean Mach numbers (1, 2 and 4) and finally the comparison with the previous idealized situations presented in paper I and a new approach to explain the formation of globules. Finally we show

Correspondence to: pascal.tremblin@cea.fr

that probability density functions of the gas can be used in observations to determine the importance of turbulence relative to the ionized-gas pressure.

## 2. Numerical methods

We used the HERACLES code<sup>1</sup> (González et al. 2007) with the ionization module described in paper I and the cooling module described in Audit & Hennebelle (2010) (based on Wolfire et al. (2003)) to model the molecular cloud and the ionization coming from the OB cluster. In addition to the physics of paper I, the turbulence in the cloud is modeled using the turbulence module described in Schmidt et al. (2006) and Schmidt et al. (2009). Gravity is an important ingredient for ultra-compact HII region (e.g. Peters et al. 2010), however we are interested in large scale HII regions (e.g. the Rosette Molecular cloud, Schneider et al. (2010). Self-gravity and the gravity from the ionizing source were considered in paper I without noticeable change on the formation of the structures. Therefore we do not consider gravity in the present study.

First, we describe the model we used for ionization. It is an

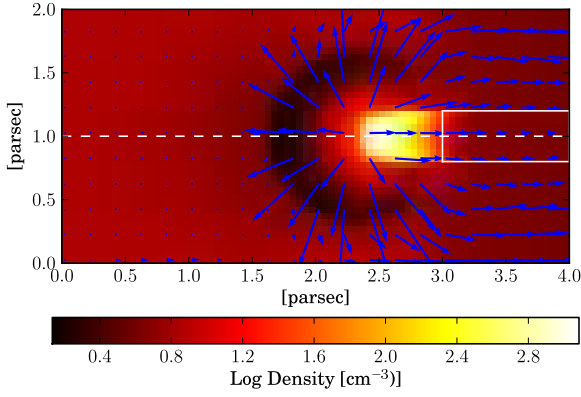


**Fig. 1.** Cut of the density field and velocity field in the radiation driven implosion of a clump inside an ionized medium. The gas behind the clump in the white box is out of equilibrium and recombines slowly. The gas at the front of the clump is escaping by the rocket effect and is cooled down by the strong expansion.

out-of-equilibrium model solving the equations

$$\begin{aligned} d(F_\gamma)/dx &= -n_H(1-X)\sigma_\gamma F_\gamma + \delta_0(x)S_* \\ d(Xn_H)/dt &= I - R = n_H(1-X)\sigma_\gamma F_\gamma - \beta X^2 n_H^2 \\ de/dt &= I \times e_\gamma - R \times k_b T / (\gamma - 1) \end{aligned} \quad (1)$$

in which  $X$  is the ionization fraction (advected with the hydrodynamic),  $F_\gamma$  is the photon flux,  $S_*$  the source term,  $n_H$  the total hydrogen density,  $\sigma_\gamma$  the cross-section for ionization,  $I$  the ionization rate,  $R$  the recombination rate,  $\beta$  is given by  $2 \times 10^{-10} T^{-0.75} \text{cm}^3/\text{s}$ ,  $e$  is the internal energy of the gas,  $e_\gamma$  the energy transferred from the ionizing photons to the electrons and  $T$  the temperature of thermal equilibrium between all the species. The first equation is the ray tracing of the ionizing photons coming from the source. The second one is the ionization/recombination photo-chemistry evolution and the third one is the thermodynamic evolution associated. 1D and 3D tests of

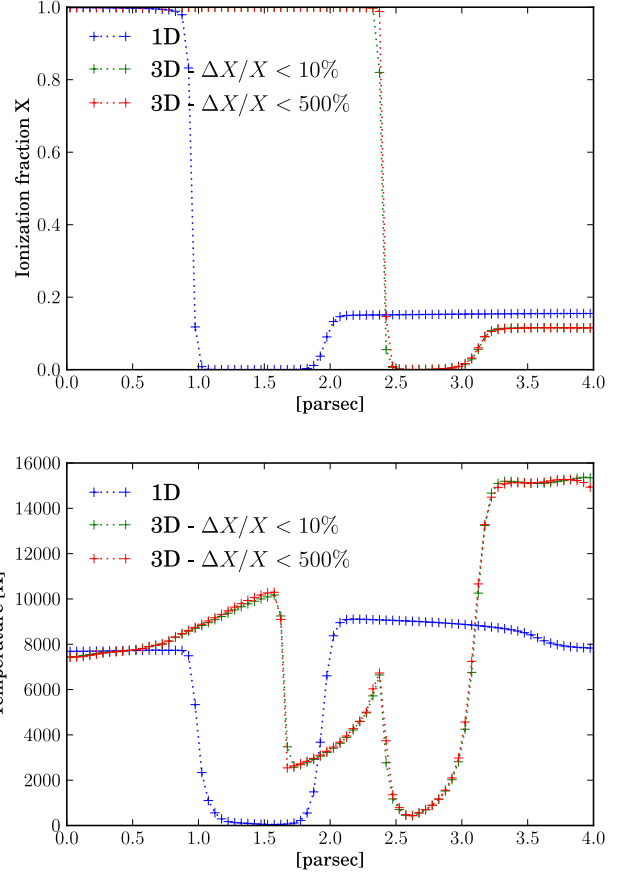


**Fig. 2.** 1D and 3D simulations of an isolated clump inside a completely ionized medium exposed to an ionization flux of  $10^9$  photons per second per squared centimeter. Note that in the 1D simulation the clump is in fact an infinite slab. Top: ionization profile through the middle of the box at  $t = 500$  ky. Bottom: Temperature profile at  $T = 500$ ky. The ionization source is at  $x = 0$  parsec. In the 1D simulation the clump is located at  $x = 1.5$  parsec while in the 3D simulations it is at 2.75 parsec. The two 3D simulations show that it is not needed to limit too much the variation of the ionization fraction. The gas behind the clump is in the shadow and is therefore being recombined. Its recombination time is long and is not at equilibrium. These simulations also show the importance of the 3D effects on the temperature structure.

the out-of-equilibrium ionization and recombination processes are performed in Sect. 3.

The turbulent forcing is modeled by an Ornstein-Uhlenbeck process in Fourier space. For each mode of the force field, random increments with a Gaussian distribution are added after each time step. The wave-numbers of the forcing modes are in the interval  $[0, 2k_0]$ , where  $k_0$  is given by the typical length scale of the forcing,  $L = 2\pi/k_0$  with  $L = 4$  pc, the size of the box in our case. By projecting the modes in transversal and longitudinal directions with regard to the wave vectors, divergence-free and rotation-free components are produced in physical space. The resulting force field is statistically homogeneous, isotropic, and stationary. The RMS magnitude is of the order  $V^2/L$ , where  $V$  is the characteristic velocity of the flow. We will perform three simulations with  $V$  resulting in stationary transonic and supersonic velocity: Mach 1, 2 and 4. The turbulence used is solenoidal with

<sup>1</sup> [http://irfu.cea.fr/Projets/Site\\_heracles/index.html](http://irfu.cea.fr/Projets/Site_heracles/index.html)

a ratio of compressive forcing power to the total forcing power of 10 %.

Three turbulent scenarii are investigated in Sect. 4, a transonic turbulent molecular cloud (mean Mach number around 1) and two supersonic cases (mean Mach number of 2 and 4). The box is a cube of 4 parsec at a resolution of 0.01 pc ( $400^3$ ), the mean density is  $500 \text{ cm}^{-3}$  and the temperature is initially at 25 Kelvin. During the turbulent evolution, the boundary conditions are periodic. The simulations are ran until a statistically steady state is obtained, i.e. a constant mean Mach number in the box. Then we turn on the ionization with a flux of  $10^9$  photons per second per squared centimeter, which is the typical flux of an O4 star at 30 parsecs. The ionization is coming from the top of the box and this face is changed to reflexive boundary condition for the hydrodynamic while the opposite side is set to free flow. The turbulent stirring is kept during the ionization phase. Some runs were done without the turbulence maintained without noticeable change, the large-scale modes do not have time to influence the small scales during the ionization phase. In Sect. 4, we investigate the interplay between turbulence and ionization for the three different simulations.

### 3. Tests of the out-of-equilibrium ionization and recombination processes

When turbulence is included in an ionization simulation, the main difference is the possibility that some ionized gas gets into the shadow of the dense ionized gas because of the mixing. This is typically an out-of-equilibrium state for the ionized gas that will begin to recombine. To study this state, we investigate simplified set-ups in which hot ionized gas is put in the shadow of dense cold gas and therefore will be out of equilibrium. We simulate the impact of ionization on a clump ( $D_{clump}=0.5$  parsec) inside an homogeneous ionized medium (see Fig. 1). We also perform an "equivalent" 1D simulation where the clump will be an infinite slab, to identify the effect of the geometry. The gas in the shadow of the clump/slab will start to recombine since it is out of equilibrium. The typical recombination time for the ionized gas is given by  $1/\beta n$  that is of the order of  $10^4$ - $10^5$  years for ionized gas at a density of  $1$ - $10/\text{cm}^3$ . It is of the order of the gas dynamical time:  $D_{clump}/c_{io} = 10^5$  years, in which  $c_{io}$  is the sound speed of the ionized gas. Therefore an out-of-equilibrium model is needed to treat this state of the gas. We studied first the profile of the ionization fraction and the effect of the limited-variation time-stepping and then the structure of the temperature in these tests.

Our method solves the two first equations in (1) implicitly while the thermal balance is solved explicitly and is sub-cycled to limit the variation of  $T$ . Usually the variation of  $X$  is limited at 10 % in the implicit step. However, it is often not needed to limit that much the variations. The ionization-fraction and the temperature profiles are plotted in Fig. 2, after 500 ky of evolution and for limited variations of 10 and 500 % and there is almost no difference between the two. At the front, the equilibrium for ionization is reached even with long time-step thanks to the implicit method, the ionization fraction is nearly at one. At the back, the recombination time of a hot ionized plasma is quite long. For example in our case the recombination time is of the order of 100 ky which also explains why the ionization fraction is still around 0.2 after 500 ky. Therefore it is possible to allow long time-steps.

We now investigate the temperature structure. The 3D profiles in Fig. 2 are taken through the middle of the box (the white-dashed line in Fig 1), therefore through the middle of

the clump, which is located between 2.5 and 3 parsecs. In the 1D case, the clump is a slab located after 500 ky between 1 and 2 parsecs. The difference of position between the two is easy to understand: in the 1D case, the ionized material cannot be evacuated on the side, the column density in front of the ionization front is higher. There are only a few ionization processes occurring at the ionization front, the dynamics is dominated by the expansion of the gas evaporating from the slab. In the 3D case, the ionized gas is escaping on the side of the clumps, therefore ionization can penetrate further inside the clump and deposit more energy. As a consequence, the clump is pushed further away by rocket motion and the energy deposit at the surface of the clump leads to a high expansion of the ionized gas and to a shock surface that can be seen in Fig. 1. The ionized gas is cooled down to 3000-6000 Kelvin by the expansion at the front.

The temperature structure is also quite different behind the clump (white box in Fig. 1) because of the shadowed recombination. In the 1D simulation, the thermal equilibrium is reached at the front, in the HII region. Behind the slab, the gas is not at equilibrium and recombines, the ionization fraction is decreasing from 1 to 0.2. The pressure drops by nearly a factor of 2 when the ionization fraction decreases from 1 to  $\approx 0.2$ . Moreover, most of the energy emitted during the recombination process is radiated away by the cooling, so that the temperature of the gas does not vary much, increasing only slightly, from  $\approx 8000$  K to  $\approx 9000$  K. The temperature structure is quite different in 3D as shown in Fig. 2. The cooling by recombination behind the clump should decrease the pressure of the gas as in the 1D case. However in 3D, it leads to lateral gas flows from the hot ionized gas exposed to the radiation to the hot recombined gas in the shadow. Therefore the recombination behind the clump is done more or less at constant pressure leading to an increase in temperature behind the clump, which is surprising at first sight.

This simple test shows that the equilibrium assumption for ionization is invalid when hot ionized gas gets in the shadow of dense ionized gas (Ionization fraction of 20 % instead of 0). The equilibrium assumption is usually justified by the fact that the recombination time is much shorter than the dynamical time. This is usually true in the HII region, however this is not the case at the interface between the HII region and the cold gas when turbulence is included. Indeed especially at high level of turbulence, hot ionized gas will be mixed with cold dense gas and therefore will be in the shadow of the cold gas, exactly in the situation we studied in this simplified test. The ionization equilibrium is not reached for a non-negligible part of the ionized gas that can get in the shadow of dense ionized gas. This is especially the case when the level of turbulence is sufficient to balance the ionized-gas pressure and to mix the unionized and ionized phases as we will see in the next section.

## 4. Turbulent simulation

### 4.1. Transonic turbulence

The first line of Fig. 3 presents three snapshots of the column density for the transonic simulation, when ionization is turned on, 500 ky and 1 My after ionization has started. The hot ionized gas expands in the cold turbulent medium and triggers the propagation of a shock ahead of the ionization front. This is the collect part of the classical collect and collapse scenario (Elmegreen & Lada 1977) and is observed in many regions (see Zavagno et al. 2010; Thompson et al. 2011; Deharveng et al.

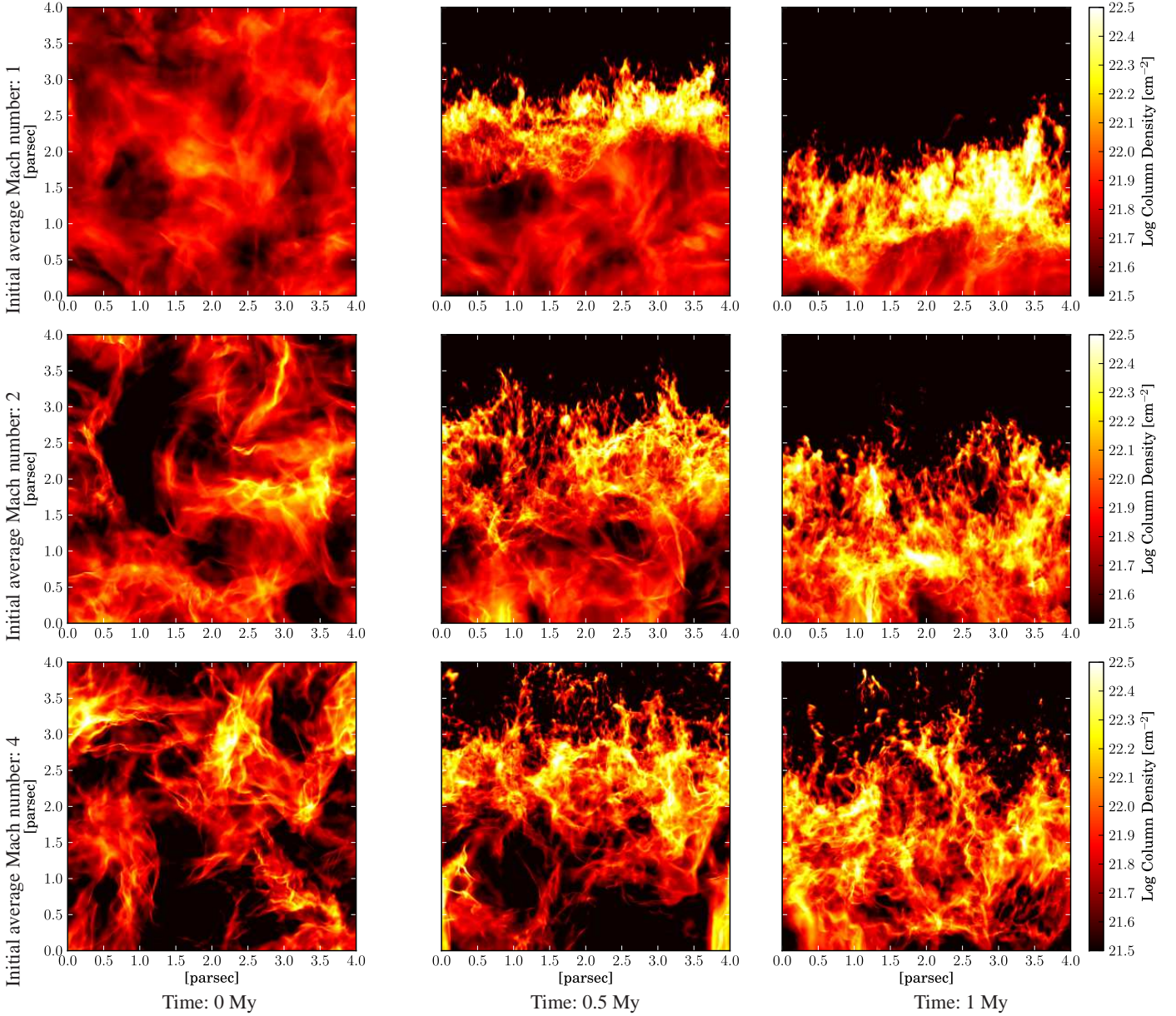


**Fig. 3.** Column density snapshots of the three turbulent simulations (row 1: Mach 1, row 2: Mach 2, row 3: Mach 4) et three different time (column 1: before ionization starts, column 2: 500 ky after ionization is turned on, column 3: 1 My).

2010). The 500-ky snapshot clearly shows a three-phase medium with the hot ionized gas at the top, the shocked dense region and the unperturbed cold cloud. The shocked region is apparently 0.5-1 parsec wide at 500 ky and gets wider in time, up to 1.5 parsec at 1 My. This width is a lot larger than one would expect from the collect process in a homogeneous medium. The typical width of the dense shell is 0.1 parsec in this case. However Fig. 4 clearly shows that the real thickness of the shell is indeed of order 0.1 parsec but contrary to the collect process in a homogeneous medium, the shell is not flat but highly curved. Therefore the column density plots show a wide shocked region just by projection effects of this highly turbulent shocked region.

The properties of these phases can be studied using the distribution of the mass fraction in the density-pressure plane or in the density-Mach number plane. Fig. 5 and 6 show the 2D plots of the mass fraction before and after ionization is turned on. Before ionization is turned on, the distribution of the gas

is at thermal equilibrium and the average Mach number is of order 1 with a dispersion of 0.48. After 1 My, the three-phase medium is formed and the three phases are well separated in the Mach number density plot. The hot ionized gas can be seen on the pressure density plot, on the isothermal equilibrium curve for the ionized gas, and on the Mach number density plot in the sub-sonic area. The unperturbed medium remains at the same location in the graph with respect to Fig. 5 while the shocked material is pushed at high Mach number and high densities. The distribution of the mass fraction is quite similar to the one found in paper I, the only difference is the initial distribution of the gas, which was previously homogeneous at  $500 \text{ cm}^{-3}$  with a density or interface modulation. In both cases, the shocked region contains points with densities higher than the one corresponding to the collect and collapse scenario (red dashed line in Fig. 5 and 6), i.e. the density after the collect phase in a homogeneous medium. These points represent 3 % of the shell in mass fraction and help

to achieve densities high enough to trigger the gravitational collapse.

#### 4.2. Supersonic turbulence and comparison

The simulations with a mean Mach number of two and four present the same three phase structures: the ionized region, the shocked region, and the unperturbed region. However, in these cases the initial gas has more turbulent ram pressure to resist the ionized-gas expansion. The pressure of the ionized gas and the ram pressure caused by turbulence can be estimated from

$$\begin{aligned} p_{II} &= 2\bar{n}_{II}k_bT_{II} \\ p_{turb} &= \rho_0v_0^2 \end{aligned} \quad (2)$$

where  $n_{II}$  and  $T_{II} \approx 7700$  K are the density and the temperature in the ionized gas and where  $\rho_0$  and  $v_0$  the density and the mean velocity in the initial turbulent medium. The density of the ionized gas is nearly constant in time in the three simulations, and does not depend on the initial turbulence.  $n_{II}$  is around  $10/\text{cm}^3$  and the corresponding pressure at  $t = 500$  ky is given in Table 1 with the initial turbulent ram pressure. The ionized-gas pressure dominates the turbulent ram pressure for a mean Mach number of one and two. The consequent progression of the ionized-gas expansion is clearly visible in the column density plots in Fig. 3. However, the plots also show that this progression is nearly stopped for a mean Mach number of four. This is caused by the fact that the turbulent ram pressure dominates the ionized-gas pressure (see Table 1). Another interesting difference between the Mach-four case and the others is the presence of many globules. It seems that the presence of these globules in our simulations can be linked with the fact that turbulent motions dominate the ionized-gas expansion, this will be investigated in more detail in Sect. 5.

Locally the ionization fraction changes from one in the ion-

**Table 1.** Initial turbulent ram pressure and ionized-gas pressure at  $t = 500$  ky

Mean Mach number	1	2	4
$p_{turb}/kb$ at $t = 0$ ky [ $\text{K}/\text{cm}^3$ ]	$3.2 \times 10^4$	$1.2 \times 10^5$	$4.5 \times 10^5$
$p_{II}/kb$ at $t = 500$ ky [ $\text{K}/\text{cm}^3$ ]	$1.7 \times 10^5$	$1.9 \times 10^5$	$1.8 \times 10^5$

ized region to zero in the unionized region in a very small zone (less than  $0.01$  pc) when turbulence can be neglected. Therefore the position at which the fraction is less than  $0.5$  gives the position of the ionization front. When turbulence is high, the position of the front is difficult to find since there is mixing between ionized gas and cold gas (see Fig. 4). However global parameters like the mean position and apparent width of the ionization front can still be studied thanks to the whole ionization fraction field. We used an average of the vertical profile of the ionization fraction. It transits between one in the completely ionized region and zero in the cold region, in between it slowly decreases because of the apparent width caused by the projection. We define the mean position of the ionizing front  $Z_X$  where the average profile is at  $0.5$  and the width  $\Delta Z_X$  as the distance between the  $0.95$  and  $0.05$  positions. This corresponds to the following equations

$$\begin{aligned} Z_X &= \int_0^{L_{\text{box}}} H(\langle X(x, y, z) \rangle_{x,y} - 0.5) dz, \\ \Delta Z_X &= \int_0^{L_{\text{box}}} H(\langle X \rangle_{x,y} - 0.05) - H(\langle X \rangle_{x,y} - 0.95) dz, \end{aligned}$$

$$H(x - y) = 1, \text{ if } x \geq y \text{ or } 0, \text{ if } x < y. \quad (3)$$

where  $X(x, y, z)$  is the ionization fraction field and  $H$  the Heavy-side function.  $Z_X$  and  $\Delta Z_X$  are shown in Fig. 7. The front progression is slowed down and its width increases as the Mach number increases. This is caused by the bigger density contrast with increasing turbulence. In the three cases, the width of the shell is mainly caused by a projection effect of the column density. The real shell is thin (see Fig. 4), but is very spatially disperse by the inner structures of the cloud. Therefore, it will look wider in column density.

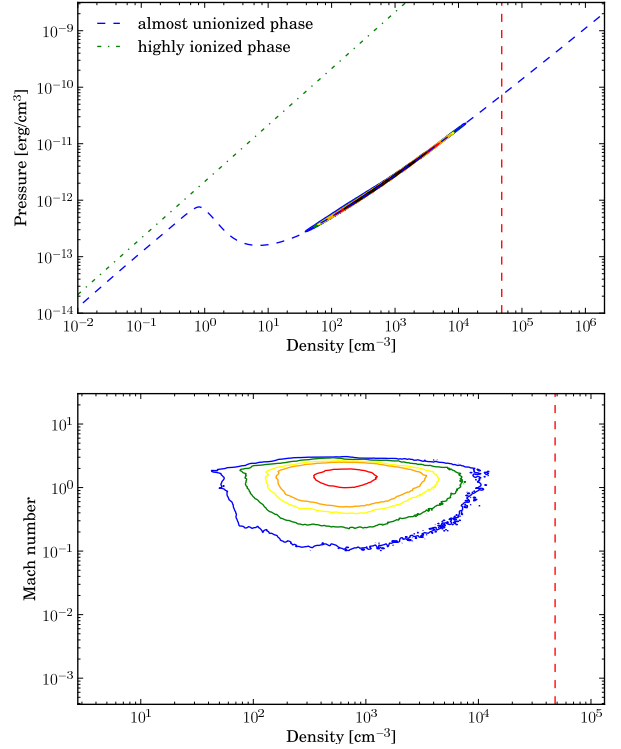


**Fig. 5.** 2D plot of the mass fraction at a given density and pressure (top) and at a given density and Mach number (bottom), before ionization is turned on in the simulation with a mean Mach number of one. Blue to black contours are increasing mass fraction contours (blue:  $1\text{E}-6$ , green:  $1\text{E}-5$ , yellow:  $5\text{E}-5$ , orange:  $1\text{E}-4$ , red:  $5\text{E}-4$ , black:  $2\text{E}-3$ ). The dashed-red line at  $4.8 \times 10^4 / \text{cm}^3$  is the maximum density achieved in a plan-parallel 1D simulation for a homogeneous density at  $500 / \text{cm}^3$ .

#### 4.3. Ionization and thermal equilibrium

The scheme we used (Sect. 2) is able to treat the ionization physics out of equilibrium. Therefore an interesting quantity to follow is the fraction of gas which is out of equilibrium. At equilibrium, the ionization rate compensates the recombination rate. From Eq. 1, the ionization fraction at equilibrium is  $X = (\sqrt{1 + 4/y} - 1)y/2$  with  $y = \sigma_\gamma F_\gamma / n_H \beta$ . In the molecular cloud  $F_\gamma$  is 0 therefore  $X$  is 0 at equilibrium. In the HII region,  $y \gg 1$  so the ionization fraction tends to 1. At the ionization front, the ionization fraction can be at equilibrium and in between 0 and 1, however this region is very small and can be neglected in the simulation (less than 1 % of the box). The

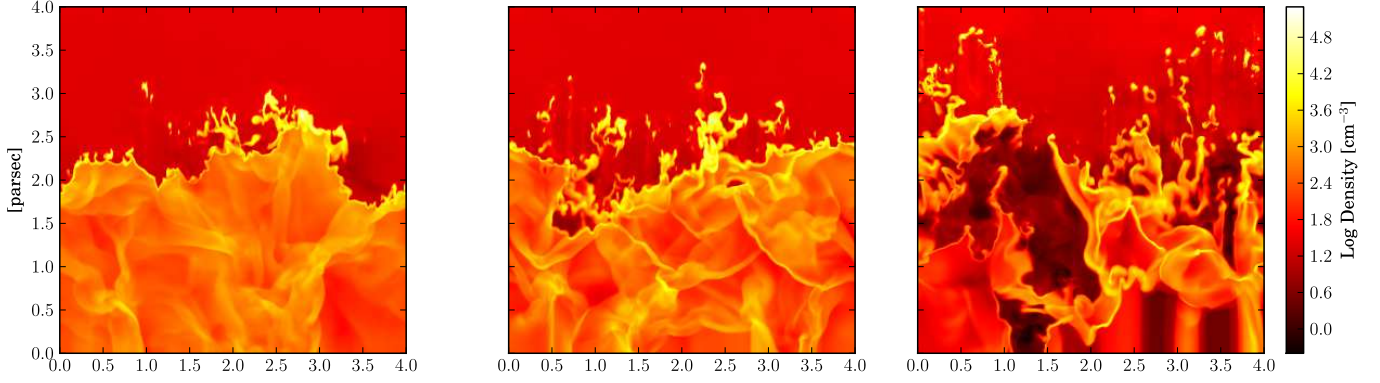


**Fig. 4.** Density cuts through the three different simulations at  $t = 500$  ky. Left: Mach 1, middle Mach 2 and right Mach 4.

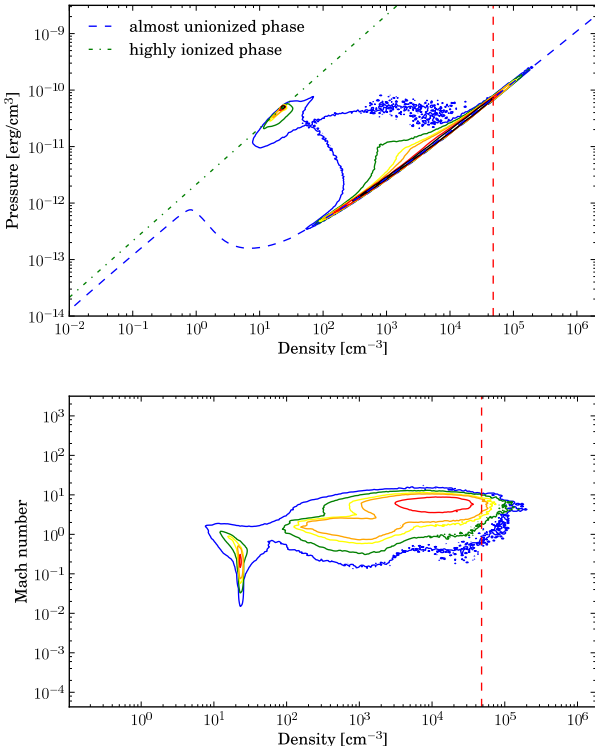


**Fig. 6.** 2D plot of the mass fraction at a given density and pressure (top) and at a given density and Mach number (bottom), 1 My after ionization is turned on. Blue to black contours are increasing mass fraction contours (blue:  $1E-6$ , green:  $1E-5$ , yellow:  $5E-5$ , orange:  $1E-4$ , red:  $5E-4$ , black:  $2E-3$ ). The dashed-red line is the maximum density achieved in a plan-parallel 1D simulation for a homogeneous density at  $500 \text{ /cm}^3$ :  $4.8 \times 10^4 \text{ /cm}^3$ .

thickness of the ionization front is given by  $1/n_H\sigma_\gamma$  which is of the order of  $10^{-4}$  pc for  $n_H=500/\text{cm}^3$ . Therefore we define the fraction of gas out of equilibrium as the percentage of cells that have a ionization fraction between 0.05 and 0.95, the values at different times for the three simulations are given in Table 2. The more turbulent the medium, the more out of equilibrium. It is interesting to note that this is similar to what was observed with the thermal instability in the interstellar medium (see Sánchez-Salcedo et al. 2002; Gazol et al. 2005; Audit & Hennebelle 2005). Almost one fifth of the simulation box at  $t = 1$  My is out of equilibrium for a mean Mach number of

four. This means that the hypothesis of an ionization equilibrium is quite bad to study the impact of ionization on a turbulent cloud. This is mainly caused by the ionized gas getting into a shadowed region. In these regions the recombination time is long, between 1 and 100 ky for densities around  $1\text{--}10 \text{ /cm}^3$  and temperature around 8000 K as we have already explained in sect. 3.

The temperature is also an important quantity to monitor in

**Table 2.** Percentage of cells out of ionization equilibrium.

Time	Mach 1	Mach 2	Mach 4
250 ky	1 %	7 %	8 %
500 ky	3 %	9 %	12 %
750 ky	5 %	10 %	13 %
1 My	6 %	12 %	17 %

our scheme. We solve the thermal balance between ionization and recombination and this allows the gas to be at states out of equilibrium as shown in sect. 2. This behavior can be identified in Fig. 8, the gas ahead of the dense parts facing the ionization flux is ionized but at a temperature between 2000 and 6000 K. This is caused by the 3D expansion of the dense ionized gas at the top of the structures facing the ionization radiation. Besides, the regions that are in the shadow of the dense structures tend to be overheated at almost 10 000 Kelvin whereas the equilibrium temperature is around 7750 Kelvin. This is caused by the fact that the recombination process in the shadow is done at constant pressure, the pressure being imposed by the hot ionized and exposed gas surrounding the shadowed gas. Therefore, as we have demonstrated in sect. 2 for the simple situation of a clump shadowing parts of the hot ionized gas, the temperature behind the clump will increase. In the turbulent simulation, the cooling processes for the unionized gas is also playing a role (see paper I for details), they will cool the recombined gas so that the temperature does not reach 14 000 Kelvin but equilibrates around 10 000 Kelvin. This result is counter-intuitive since one would expect that the gas stays at 7750 Kelvin during the recombination step, the kinetic energy of the electrons being radiatively lost for the system. However, the 3D versus 1D study done in sect. 2 clearly show the importance of the lateral motions from the exposed gas to the shadowed gas to impose a recombination at constant pressure behind the structures.

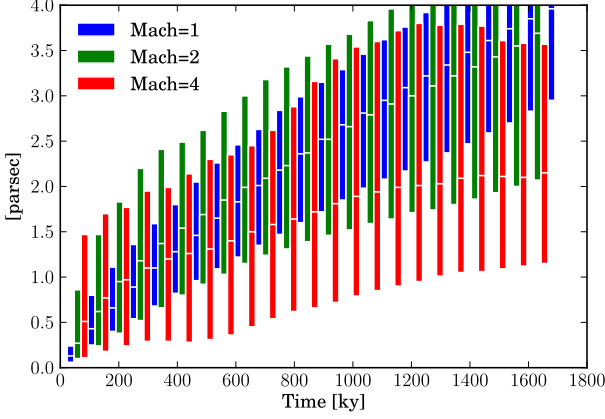


**Fig. 7.** Positions of the 0.95-, 0.5- and 0.05-transition of the xy-average ionization fraction. Between 0 and the lower bound the ionization fraction of the gas is between 1 and 0.95, between the lower bound and the middle bound, between 0.95 and 0.5 and between the middle bound and the upper bound the ionization fraction is between 0.5 and 0.05.

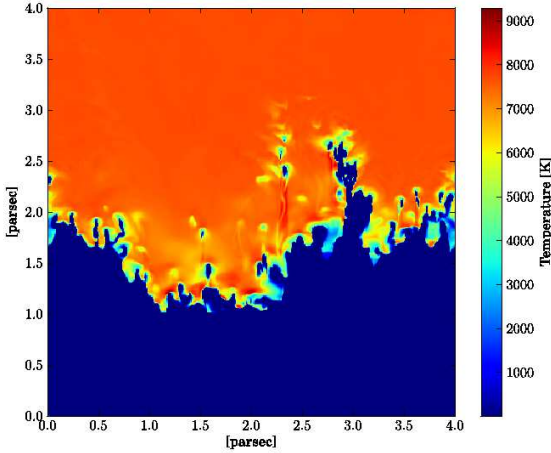


**Fig. 8.** Temperature cut at  $t \approx 710$  ky after ionization is turned on. The 3D temperature effects studied in the clump simulation (sect. 2 are clearly visible through the snapshot.

## 5. Structures and observational signatures

### 5.1. Pillars

It is not clear how to distinguish structures on the column density maps in Fig. 3 because of the confusion on the line of sight. Therefore we will investigate some density cuts to identify pillars and globules. Figure 9 presents the formation of a pillar in the Mach 1 simulation between 200 and 700 ky. The pillar formed is one parsec long and presents a complex structure, with successive dense parts along its length. Figure 10 is a map along the pillar with the direction of the velocity field. The structure of the field is similar to the one already obtained in paper I for non-turbulent set-ups. The pillar has two dense heads at a vertical position of 1.4 and 1.6 parsec, a dense base between 1.8 and 2 parsec and two holes on the side at 2.4 parsec. The velocity field shows that the pillar is forming at its base by the convergence of the dense parts of the shell while the holes are formed by the divergence of the dense parts

created on a concave zone. This is the same configuration that was previously seen in paper I, without any turbulence. This suggests that the mechanism at the origin of the formation of pillars are not too much dependent on the turbulence. Here the turbulence gives only the initial conditions in terms of density contrasts and initial structures on which pillars will form. The holes on the side of the pillars in the non-turbulent set-ups of paper I were in fact a complete annulus around the pillars caused by the symmetry of our initial conditions. The major difference with a turbulent scenario is that there is no more symmetry in the initial conditions. This leads to holes that are local and do not extend in a full annulus.

The curvature of the shell can also be seen on spectra

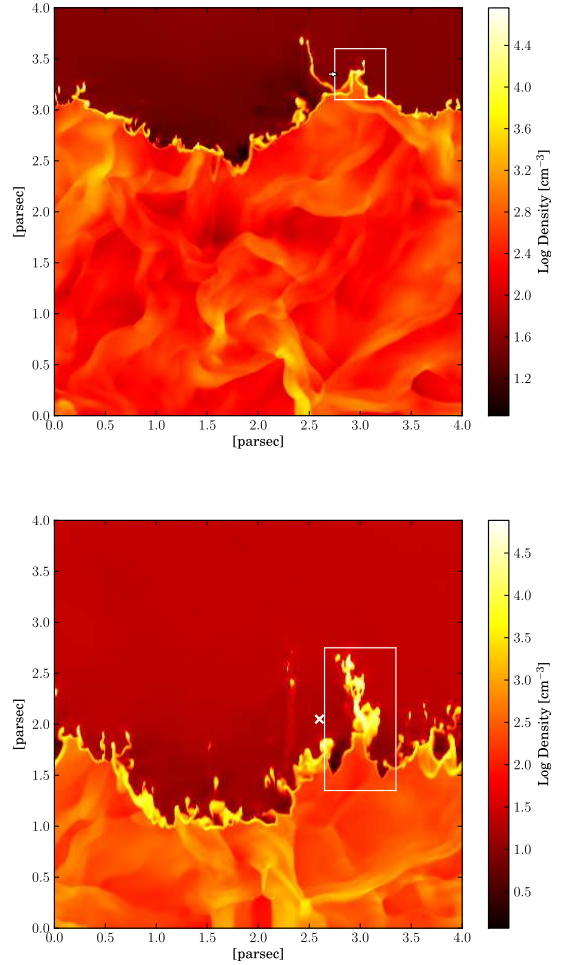


**Fig. 9.** Density cut at  $t \approx 240$  ky and  $t \approx 710$  ky after ionization is turned on. The white box indicates the areas of the column density and line-of-sight velocity spectra made in Fig. 11 and 12. The arrow indicates the direction of the line of sight; for the cross, the line of sight is perpendicular to the density cut plane.

of the line-of-sight velocity. Figures 11 and 12 show on the left a column density maps of the pillar and on the right the mass histograms as a function of the line-of-sight velocity in squares of 0.05 parsec. Figure 11 is a snapshot at  $t \approx 240$  ky when the pillar is not yet formed and Fig. 12 at  $t \approx 710$  ky with the whole pillar. The line-of-sight velocity spectra are wide (between -2 and +2 km/s) before the pillar is formed. This was

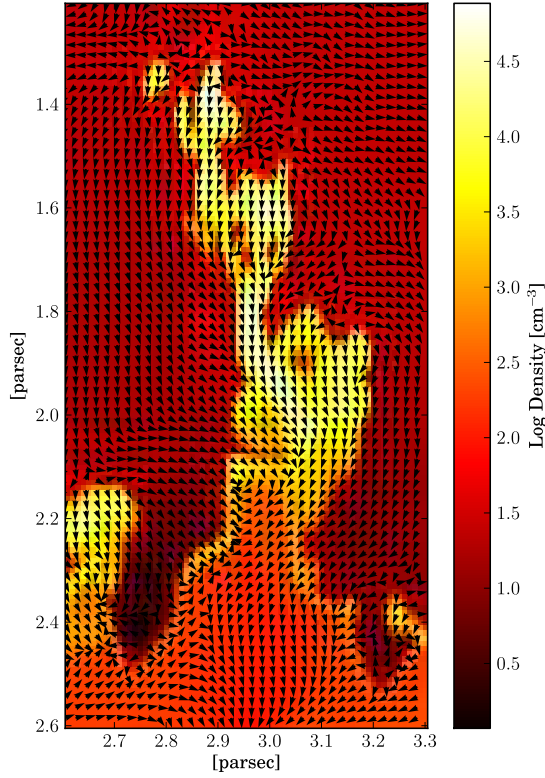


**Fig. 10.** Cut of density field and velocity field orientation along the pillar at  $t \approx 710$  ky.

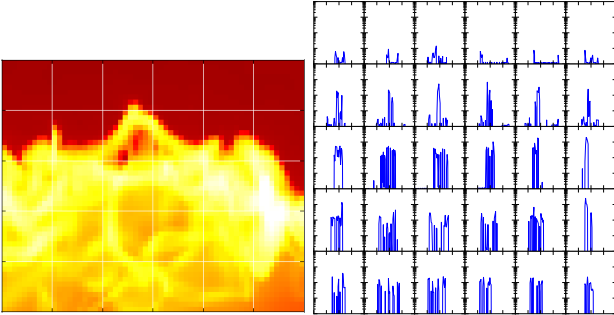


**Fig. 11.** Left: column density on a  $0.6 \times 0.5 \times 0.5$  pc<sup>3</sup> box around the area in which the pillar will form at  $t \approx 240$  ky. Right: mass-weighted histogram of the line of sight velocity in the same box (similar to optically-thin observational line spectra). Each spectrum is made on a square of  $0.1 \times 0.1$  pc<sup>2</sup> drawn on the column density map. The spectra are drawn between  $-4$  and  $4$  km/s in 80 bins (horizontal axis) and the mass between  $10^4$  and 1 solar mass (vertical axis in log scale). The lateral shocks can be identified in the wide spectra leading to a very broad averaged line width.

already identified in paper I as the signature of the dense shell which is curved on itself with the two components, blue-shifted and red-shifted, that are going to collide to form the pillar. When the collision has occurred, the wide spectra is no longer visible and the line-of-sight velocity spectra are peaked around a null velocity (see Fig. 12). This demonstrates that the scenario identified in paper I with the study of non-turbulent set-ups is

also taking place in our turbulent simulation.

Based on this analysis, we can infer that molecular tracers

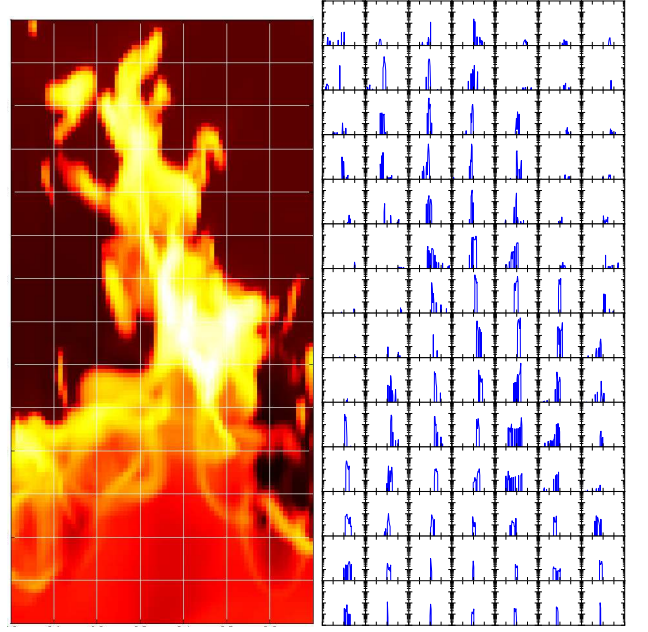


**Fig. 12.** Left: column density on a  $0.7 \times 1.4 \times 0.5$  pc<sup>3</sup> box around the pillar structure at  $t \approx 710$  ky. Right: mass-weighted histogram of the line of sight velocity in the same box (similar to optically-thin observational line spectra). Each spectrum is made on a square of  $0.1 \times 0.1$  pc<sup>2</sup> drawn on the column density map. The spectra are drawn between  $-4$  and  $4$  km/s in 80 bins (horizontal axis) and the mass between  $10^4$  and 1 solar mass (vertical axis in log scale). The lateral shocks have collided to form the pillar, the spectra are now peaked around 0 km/s.

that are optically thin should reflect the same spectral structure as the line-of-sight velocity spectra of the simulations. Therefore, wide spectra could be the indication of nascent pillars whereas evolved pillars should present a spectra peaked around the velocity of the expanding bubble projected on the line of sight. This velocity is zero in our case since the line of sight is perpendicular to the direction of the expansion.

### 5.2. Dense clumps at the edge of the ionized gas

The difference between the formation mechanism of pillars and clumps inside the shell is also clearly visible in Fig. 9. On the first snapshot the position on which the pillar is forming can be identified as the position at which the curvature of the shell is higher. On the other parts of the shell, the curvature is not sufficient to form pillars but will rather trigger the formation of clumps inside the shell. This phenomenon was already seen in Paper I, the higher the curvature, the longer the pillar. If the shell is curved enough to collapse on itself it will form a pillar. At high curvature, the tip of the curved shell will be stopped by the collapse of the matter ahead of it, which leads to the formation of a pillar (Right part of Fig. 13, at early times the velocity field of the shocked gas shows that the shell collapses on the centre of the initial structure). The shell around the “hill” will collapse quickly on the hill, with velocities that are nearly perpendicular to the direction of the expansion. That is why the motion of the gas at the top of the hill is small. When the curvature is



low, the shell collapse on the hill but with a velocity that has a component in the direction of the expansion. Therefore after the collapse, the shocked gas keeps a velocity in the direction of the expansion and propagates with the rest of the shell. The matter is accelerated with the shell and the density increases because the gas surrounding it converges smoothly at the centre (Left part of Fig. 13). This situation was studied and compared in the context of RCW36 in Vela C molecular cloud (see Minier et al. 2012 in prep). The new observations from the Herschel space telescope show the presence of dense clumps around the HII region RCW36. Dedicated numerical simulations show that it is rather unlikely that these clumps were pre-existing because they would have triggered the formation of pillars. These dense clumps are located at the edge of the HII region and therefore they are formed by the lateral flows in the shell caused by curvature perturbations that are not high enough to form pillars. It is exactly the same process that is at work in the present turbulent simulations. From paper I, it can be estimated that the transition from clump to pillar formation is at a curvature radius between  $2.5 \times 10^{-2}$  and  $5 \times 10^{-2}$  pc in the present situation.

Thompson et al. (2011) showed that the dense clumps around HII regions are preferentially located at the interface between the ionized gas and the cold gas. We propose here a formation mechanism of these dense clumps in the shell thanks to curvature perturbations. However if the turbulent ram pressure dominates the ionized gas pressure, such dense clumps will not be present exactly at the interface. The cold gas as sufficient kinetic energy to disrupt the interface and a mixing region between the dense shocked gas and the ionized gas is present (see Fig. 4). Therefore the clear correlation in the observations between the position of the dense clumps and the interface suggests that in most of these regions the ionized-gas pressure dominates the turbulent ram pressure of the surrounding gas.

### 5.3. Globules

Contrary to the dense clumps in the shell, globules are bubbles of gas disconnected from the molecular cloud and surrounding by ionized gas. The major difference between the turbulent simulations presented in this paper and the non-turbulent set-ups studied in paper I is the appearance of these globules in the highly turbulent case. As we have already discussed above, globules emerge because the ram pressure of turbulence dominates the pressure of the ionized gas. These bubbles of cold dense gas have enough kinetic energy to penetrate inside the HII region. An interesting consequence is that the motion of the globules is imposed by the turbulence. They could have by chance a motion aligned with the direction of expansion of the HII region but most of the time, they should have a random motion direction set by the turbulence, and it is indeed the case in our simulation. The direction of expansion of the HII region is from top to bottom in Fig. 3. Therefore projected on the line of sight which is perpendicular, the velocity in the expansion direction is zero. The motion of a pillar is typically aligned with the direction of expansion of the HII region, as it can be seen on Fig. 12. The spectra are centered at zero. However it is not the case for a globule. Figure 14 shows a typical globule in the simulation at Mach four. The line-of-sight velocity spectra are systematically shifted at a velocity of +4 km/s which is of the order of ten times the sound speed of the cold gas. The shift is also highlighted in Fig. 15. The globule does not have a motion aligned with the direction of expansion. In a region where globules and pillars are present, the velocity of a pillar is the velocity of expansion of the front projected on the line of sight, whereas the velocity of a globule will

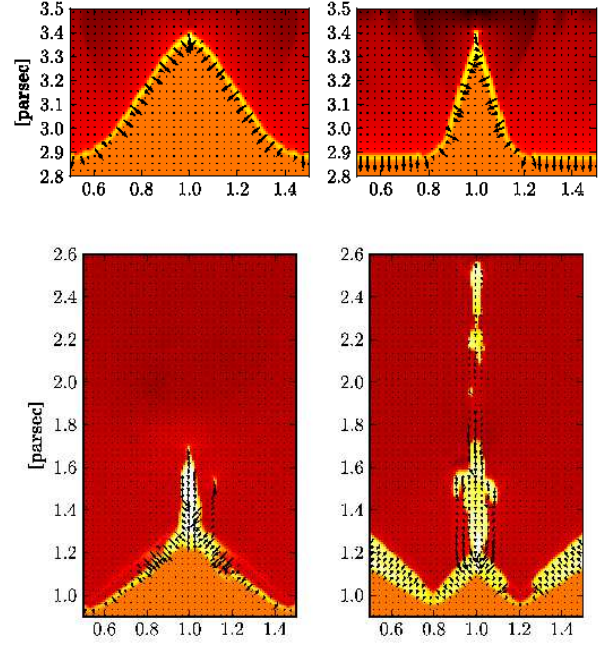


**Fig. 13.** Illustration of the effect of the shell curvature on the formation of clumps and pillars. Density cut and velocity field (for the ionized gas) are taken from simulations from paper I. Initial curvature radius: left:  $5 \times 10^{-2}$  pc and right:  $1 \times 10^{-2}$  pc. Top: 20 ky after the beginning of the simulation, the shell is formed on the curved surface. Bottom: snapshots after 550 ky. A 1.5-pc long pillar is formed at high curvature whereas a clump of the size of the initial structure is formed at low curvature.

be the signature of the initial turbulence. The dense clumps that are observed in the shell also move with the expansion of the HII region. Therefore the same velocity shift between these clumps and the globules nearby can be expected. In that picture, pillars and clumps at the edge of the HII region are the result of a structure dominated by the ionization dynamics whereas globules are turbulent dominated. This is quite different from the radiation driven implosion scenario, in which there is no reason for the globules to have a velocity different from pillars.

This signature of the turbulent nature of a globule is supported by recent observations in the Cygnus X region. Thanks to Herschel Open Time and SOFIA observations (Schneider et al. 2012b),  $138 \mu\text{m}$  and CO maps are available and contain several pillars and globules. A pillar and a globule in this region were identified to be sufficiently close (and the HII region sufficiently big) to consider they should have the same direction of motion if the motion is only imposed by the HII region expansion. However the [CII] spectra show a line-of-sight velocity difference of two kilometers per second, which is clearly supporting a turbulent scenario for the formation of the globule against the radiation implosion of an isolated clump.

The difference of 2 km/s is therefore an indication of the level of initial turbulence. For a sonic velocity of 0.4 km/s, this shift indicates typically a motion at Mach 5. In our simulation, the globule is at Mach 10 whereas the mean Mach number of the simulation is 4. Therefore the velocity of the globule is an indication of the turbulence level but not a precise measurement.

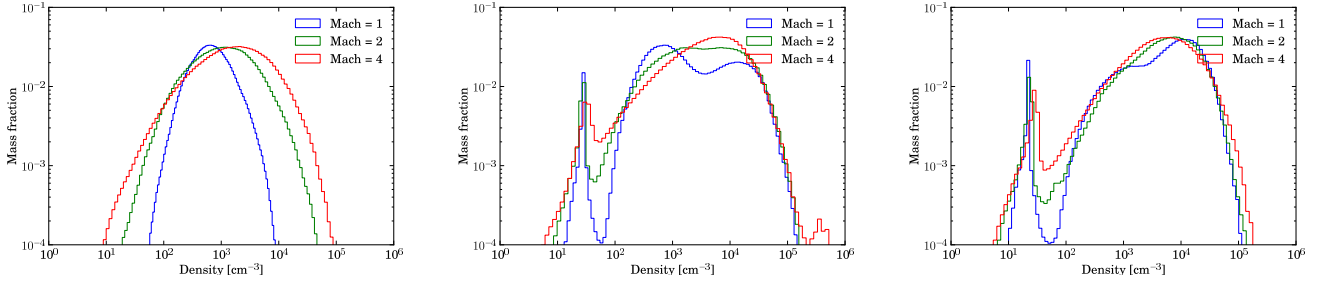


**Fig. 16.** Probability density function of the gas for the three simulations. Left:  $t = 0$  ky, middle:  $t = 500$  ky, right:  $t = 1$  My. The first peak is the ionized gas and therefore is not seen in the observations. At  $t = 500$  ky, the Mach-1 simulation presents a double peak, the first one corresponds to the unperturbed turbulent gas, the second one to the shocked region. In the Mach-2 simulations, the peak is barely visible because the turbulence is higher and because the unperturbed region still present in the box becomes small. In the Mach-4 simulation, the turbulence is too high, and the second peak is hidden in the peak of the turbulent cold region.

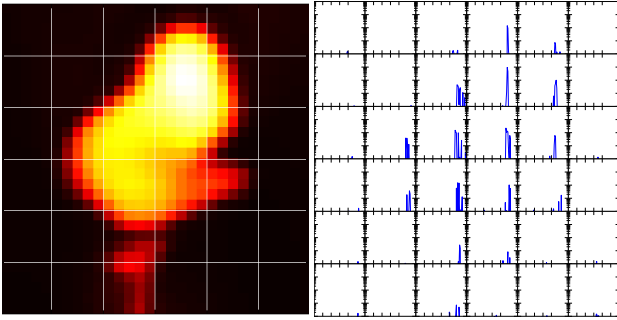


**Fig. 14.** Left: column density on a  $0.3 \times 0.3 \times 0.25$  pc<sup>3</sup> box around a globule in the Mach 4 simulation. Right: mass-weighted histogram of the line of sight velocity in the same box (similar to optically-thin observational line spectra). Each spectrum is made on a square of  $0.05 \times 0.05$  pc<sup>2</sup> drawn on the column density map. The spectra are drawn between  $-6$  and  $6$  km/s in 80 bins (horizontal axis) and the mass between  $10^4$  and 1 solar mass (vertical axis in log scale). All the spectra are red-shifted at a velocity of  $+4$  km/s.

#### 5.4. Probability density function

In this section, we investigate the density structure of the gas using probability density functions (PDFs). Numerical models (e.g. Kritsuk et al. 2007; Audit & Hennebelle 2010; Ballesteros-Paredes et al. 2011) and observations of atomic and molecular gas (e.g. Kainulainen et al. 2009) show that PDFs are log-normal at low densities and can have more complex shapes at higher densities. We here plot the mass fraction against the density (Fig. 16) from our simulations in a temporal evolution and obtain that the PDF shape depends on turbulence and time. At low turbulence (Mach 1) the probability density function is double-peaked because of the ionization, similarly to the bimodal PDFs caused by the thermal instability (see Sánchez-Salcedo et al. 2002; Gazol et al. 2005; Audit & Hennebelle 2005). The dense compressed gas is forming a new peak in the distribution. At high turbulence, the probability density function is shifted toward higher densities but does not present the double peak. This directly tells that a double peak is the signature of a region dominated by the ionization whereas a single peak is the signature that the turbulence is dominant. This signature was already observed in the Rosette nebula by Schneider et al. (2012a). The PDFs at the edge of the HII regions present the same double-peaked signature. It suggests that at the border of the bubble, the turbulence is low compared to

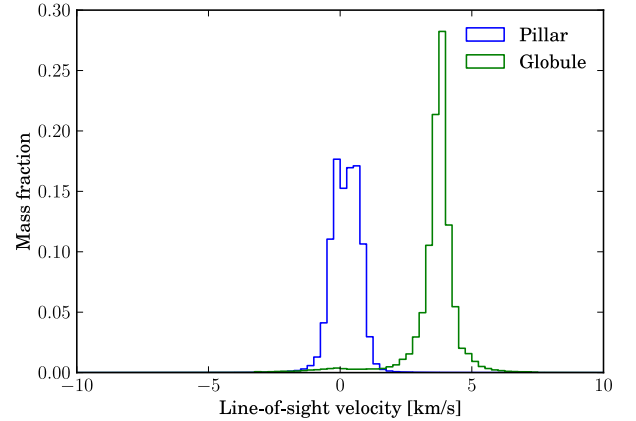


**Fig. 15.** Mass fraction of the gas in the pillar and in the globule in function of the velocity. The bulk line-of-sight velocity of the pillar is at  $0$  km/s whereas the bulk velocity of the globule is at  $+4$  km/s.

the ionized-gas pressure.

Based on the PDFs of the Mach 2 simulation, it is clear that the double peak disappears when there is no more unperturbed gas in the region on which the PDFs are done. Therefore a good way to look at the PDFs around a HII region is to do concentric PDFs centered on the central ionizing cluster. By increasing the radius of the region, we will first capture the peak of the shocked region, then a double peak should appear when the unperturbed region is included. Then the first peak should disappear at some point, when the shocked region becomes negligible compared to the unperturbed region. This point could indicate on which scale the central cluster has an impact on the global PDF of the cloud and therefore on which scale, the initial mass function is impacted by the ionization. If the turbulence is high, it is possible that the shocked peak is hidden in the large peak of the turbulent cloud. In that case, no double peak will appear and this will be an indication that the turbulence in the region dominates over the ionized-gas pressure.

## 6. Conclusions

Structures at the interface between HII regions and molecular clouds can be classified mainly in three categories: pillars, globules and dense clumps. Various scenarios have been investigated in the past to explain their formation: collect & collapse, radi-

ation driven implosion, shadowing effects and turbulence. We presented a new model to explain the formation of clumps and pillars in paper I based on the curvature of the dense shell formed by the collect processes. High curvature leads to pillars, low curvature to instabilities forming dense clumps and dips in the shell. This model was investigated using non-turbulent set-ups. In the present paper we show that the same mechanisms are at work in simulations with a turbulent cloud. Especially the same spectral observational signatures can be identified on the formation stages of the pillars.

Furthermore we have shown that:

- Because of turbulence, hot ionized gas can get into the shadow of cold dense gas, leading to a very long recombination time for the gas. This gas can only be treated with a non-equilibrium model for ionization, up to 20 % of the box can get into that state. The equilibrium assumption is valid in situations in which the ram pressure of turbulence is not dominating the ionized-gas pressure, i.e. low turbulence levels.
- Globules are formed preferentially when the turbulence in the cold gas dominates the ionized-gas pressure. Bubbles of dense gas have sufficient kinetic energy to penetrate into the HII regions forming the globules. A signature of this scenario is the line-of-sight velocity spectrum of the globules which is either blue-shifted or red-shifted compared to the spectrum of a pillar or a clump at the edge of the HII region. This can be directly observed in regions where pillars, clumps and globules are present.
- Probability density functions are double peaked when the turbulent ram pressure is low compared to the ionized-gas pressure. They could be used in observations as probes to determine the relative importance of the turbulence compared to the ionization.

An important step now is to do the statistics of the formation of dense structures at the edge of HII regions. It will be of great importance to conclude on the potential negative or positive effects of radiative feedback on the star-formation rates. Furthermore comparisons with observations will also tell how realistic the curvature scenario for the formation of dense clumps and pillars and the turbulent scenario for the formation of globules are.

## References

Arthur, S. J., Henney, W. J., Mellema, G., De Colle, F., & Vázquez-Semadeni, E. 2011, *MNRAS*, 414, 1747  
 Audit, E. & Hennebelle, P. 2005, *A&A*, 433, 1  
 Audit, E. & Hennebelle, P. 2010, *A&A*, 511, 76  
 Ballesteros-Paredes, J., Vázquez-Semadeni, E., Gazol, A., et al. 2011, *MNRAS*, 416, 1436  
 Bertoldi, F. 1989, *ApJ*, 346, 735  
 Dale, J. E. & Bonnell, I. 2011, *MNRAS*, 414, 321  
 Dale, J. E., Bonnell, I. A., Clarke, C. J., & Bate, M. R. 2005, *MNRAS*, 358, 291  
 Deharveng, L., Schuller, F., Anderson, L. D., et al. 2010, *A&A*, 523, 6  
 Elmegreen, B. G. & Lada, C. J. 1977, *ApJ*, 214, 725  
 Gazol, A., Vázquez-Semadeni, E., & Kim, J. 2005, *ApJ*, 630, 911  
 Gerin, M., Goicoechea, J. R., Pety, J., & Hily-Blant, P. 2009, *A&A*, 494, 977  
 González, M., Audit, E., & Huynh, P. 2007, *A&A*, 464, 429  
 Gritschneider, M., Burkert, A., Naab, T., & Walch, S. 2010, *ApJ*, 723, 971  
 Hester, J. J., Scowen, P. A., Sankrit, R., et al. 1996, *Astronomical Journal* v.111, 111, 2349  
 Kainulainen, J., Beuther, H., Henning, T., & Plume, R. 2009, *A&A*, 508, L35  
 Kritsuk, A. G., Norman, M. L., Padoan, P., & Wagner, R. 2007, *ApJ*, 665, 416  
 Lefloch, B. & Lazareff, B. 1994, *A&A*, 289, 559  
 Mackey, J. & Lim, A. J. 2010, *MNRAS*, 403, 714  
 Mellema, G., Arthur, S. J., Henney, W. J., Iliev, I. T., & Shapiro, P. R. 2006, *ApJ*, 647, 397

Peters, T., Mac Low, M.-M., Banerjee, R., Klessen, R. S., & Dullemond, C. P. 2010, *ApJ*, 719, 831  
 Sánchez-Salcedo, F. J., Vázquez-Semadeni, E., & Gazol, A. 2002, *ApJ*, 577, 768  
 Schmidt, W., Federrath, C., Hupp, M., Kern, S., & Niemeyer, J. C. 2009, *A&A*, 494, 127  
 Schmidt, W., Hillebrandt, W., & Niemeyer, J. 2006, *Computers & Fluids*, 35, 353  
 Schneider, N., Csengeri, T., Hennemann, M., et al. 2012a, *A&A* accepted  
 Schneider, N., Güsten, R., Tremblin, P., et al. 2012b, *A&A* accepted  
 Schneider, N., Motte, F., Bontemps, S., et al. 2010, *A&A*, 518, L83  
 Thompson, M. A., Urquhart, J. S., Moore, T. J. T., & Morgan, L. K. 2011, arXiv, astro-ph.GA  
 Tremblin, P., Audit, E., Minier, V., & Schneider, N. 2012, *A&A*, 538, 31  
 Williams, R. J. R. 1999, *MNRAS*, 310, 789  
 Wolfire, M. G., McKee, C. F., Hollenbach, D., & Tielens, A. G. G. M. 2003, *ApJ*, 587, 278  
 Zavagno, A., Russeil, D., Motte, F., et al. 2010, *A&A*, 518, L81